JOURNAL OF MULTIFUNCTIONAL MATERIALS & PHOTOSCIENCE
12(1), June 2021, pp. 25-55

Purification, dissociation, modification and application of palygorskite : A review

Sheng Wang[a], Yin Liu[a, b, c,*], Tianshu Zhang[a] and Ling Bing Kong[d,*]

Sheng Wang[a], Yin Liu[a, b, c,], Tianshu Zhang[a] and Ling Bing Kong[d,*]*
[a]School of Materials Science and Engineering, Anhui University of Science and Technology, Huainan 232001, Anhui, China
[b]State Key Laboratory of Mining Response and Disaster Prevention and Control in Deep Coal Mines, Anhui University of Science and Technology, Huainan 232001, Anhui, China
[c]Anhui International Joint Research Center for Nano Carbon-based Materials and Environmental Health, Anhui University of Science and Technology, Huainan 232001, Anhui, China
[d]College of New Materials and New Energies, Shenzhen Technology University, Shenzhen 518118, Guangdong, China

Abstract: Palygorskite is a natural clay mineral, with excellent properties, owing to its special crystal structure. Natural palygorskite is non-toxic and cost-effective, making it potential for a wide range of applications. However, natural palygorskite contains various associated minerals, which should be purified before it is used for real applications. Although progress has been made in recent years, almost no overview information is available in the open literature. In this review article, we aimed to summarize the recent progress in purification, modification and application of palygorskite. The advantages and disadvantages of the different purification and modification methods will be briefly discussed. The applications will be focused on pollution treatment, photocatalysts and microwave absorption. Finally, conclusions will be listed and perspectives will be provided.

Keywords: Palygorskite, Purification/dissociation, Modification, Adsorbent, Photocatalyst, microwave absorption.

1. Introduction

Palygorskite (Pal), also known as attapulgite, is an aquo-magnesium-rich aluminosilicate clay mineral, with a chain-layer structure. the crystal structure of palygorskite is shown in Fig. 1 [1]. There is a layer of magnesium (aluminum)-oxygen (hydrogen-oxygen) octahedron in between two silicon-oxygen tetrahedrons (ribbons of 2:1 phyllosilicate modules), unlike other layered silicates, they lack continuous octahedral sheets [2, 3]. Therefore, the basic structural characteristics of Pal are very obvious, including: continuous tetrahedral layer; pyroxene like chain formed by inverted tetrahedron arrangement; and discontinuous octahedral layer [3-5]. The discontinuous (Mg, Al)-(O, OH) octahedral ribbons are inversely connected by Si-O-Si bonds to form a channel structure of approximately 0.37×(0.60-0.56)×1.10 nm width [6]. In addition, Pal exhibits

* Corresponding author*: yinliu@aust.edu.cn; konglingbing@sztu.edu.cn*

a unique fibrous or rod-shaped structure due to the inversion of oxygen atoms at the edge of the Si-O tetrahedral layer [7]. Generally, the crystal structure of Pal has three levels. The primary level is fibrous or rod-like single crystal, with an average diameter of 10 nm and lengths of 0.1-1 ìm. Then, rod single crystals are arranged in a close parallel manner to form rod beams. The rod beams could be packed or stacked in different ways to obtain rod aggregates [8, 9]. In theory, the chemical formula of Pal is (Mg, Al, Fe)$_5$Si$_8$O$_{20}$(OH)$_2$(OH$_2$)$_4$·4H$_2$O. However, due to the isomorphic substitution phenomenon in the formation of natural Pal, the actual structural formula is different from the theoretical one. Generally, Al^{3+}, Fe^{2+}, Fe^{3+} and a small amount of transition metal ions can occupy the octahedral position of Mg^{2+}. Octahedral cations in Pal are usually located in the center of inner and marginal octahedron. The specific location is shown in Fig. 1. With these interesting features, Pal displays various special physical and chemical properties, such as unique rheological characteristics, cation exchange capability, adsorbability and carrier properties. Therefore, Pal could have a wide range of applications in chemical engineering, building materials, medicines, catalyst support, dyes adsorbent and so on [10-13]. However, the rod-shaped crystals of natural Pal tend to aggregate as crystal bundles due to the van der Waals force and hydrogen bonds. In addition, there are often impurities in natural Pal, such as, dolomite, quartz and montmorillonite. The presence of the aggregation and these impurities would greatly weaken the nano characteristics of Pal, especially its carrier performance. As a result, in order to make full use of Pal, it is necessary to purify and dissociate the original ores.

Although significant progress has been made in the purification, modification and application of Pal, it has been rarely overviewed in the open literature. In this regard, we attempted to summarize purification technologies, modification methods, new applications of adsorption, photocatalysis and microwave absorption for Pal, which have been reported in recent years.

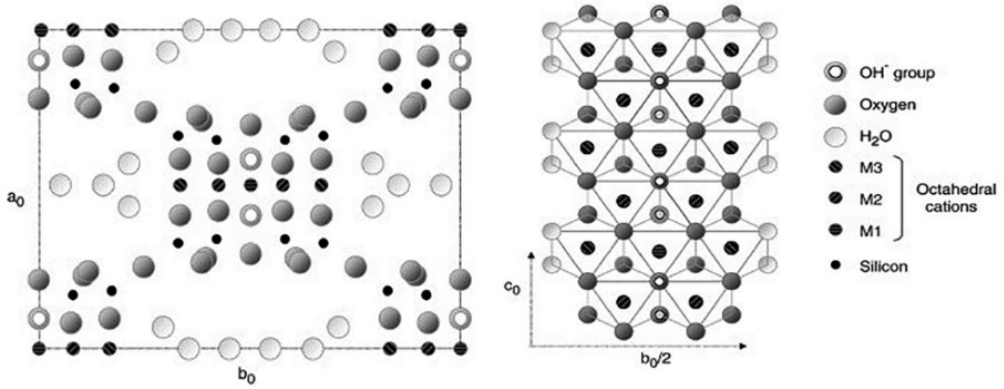

Fig. 1. Structures of palygorskite projected on (001) and octahedral ribbon [1].

2. Method study

2.1 Purification

At present, two main methods are used to purify and dissociate Pal: dry method and

wet method. Dry method, which is simple and cost-effective. Then, the gravity difference is used to separate the clay particles. However, the clays purified in this way have relatively low quality, with properties far below the requirements of fine chemicals industries, such as adsorbents in cosmetics and drug carriers in medicines. Accordingly, the purification of Pal has mainly focused on wet method. Wet purification is a multiple step process, including crushing and soaking of the original ores, mechanical stirring and ultrasonic treatment with or without dispersant, separation and removal of impurities through centrifugation or sedimentation and pressure filtration drying. In the process of wet purification, the solvent can enter the gap of the Pal aggregates, change the surface charge of the rod crystals, dissolve the soluble impurities and maintain the aspect ratio and crystal structure of the Pal to the greatest extent. Compared with the products obtained by using dry method, the Pal dissociated by using wet purification showed much improved properties. In wet method, it is very important to select the solvents, dispersing agents and slurry ratios [14].

Although these simple methods could separate the impurities, such as dolomite and quartz, the purification efficiency was relatively low. Besides, the single chemical purification method encountered not only high cost, but also secondary pollution risk. Accordingly, the purification of Pal has been mainly focused on the combination of physical and chemical ways. High purification efficiency could be readily achieved, by optimizing the parameters, such as dispersant type and quantity, acid content and acidification time, mixing time and centrifugation speed.

Common dispersants include sodium silicate, sodium pyrophosphate, sodium hexametaphosphate, polyacrylic acid, and sodium polyacrylate, since they all have a strong electrostatic interaction with the negative electric potential of the Pal surface. With the presence of an effective dispersant, the dispersity of Pal is enhanced and hence the surface impurities are easily separated. Strong acids, such as hydrochloric acid, nitric acid and sulphuric acid, are usually used in the purification of Pal. The acids mainly aid to dredge the channels and separate the impurities, which together with the cooperation with the effects of dispersant and mechanical action are responsible for the high purification efficiencies.

2.2. Dissociation

The traditional methods for the dissociation of Pal bundles mainly include shear, impact, grinding, ball milling, extrusion and so on [14].

Boudriche et al. studied the effect of dry milling processes on the surface properties of Pal [15]. Among the tested dry grinding devices, grinding in an air jet mill (Alpine 50 AS) and a vibratory ball mill (Pulverisette 0) led to the most significant particle size reduction. The results showed that the damage of Pal rod crystal structure was not obvious in short time grinding. After grinding for a long time, the rod crystal of the Pal was broken, even the fiber morphology was completely destroyed, resulting in agglomeration. Moreover, due to the destruction of the channel structure of Pal, the

specific surface area decreased from 114.5 m^2/g to 62.6 m^2/g. However, the results showed that whatever the grinding process, the microstructure of Pal was not affected.

3. Results and discussion

3.1 Properties and Dissociation

Liu et al. investigated that the effects of dry grinding treatment on the morphology, crystal structure, specific surface area, pore structure of Pal [16]. The results showed that the dry grinding treatment could dissociate the crystal bundles of Pal, but the aspect ratio of rod-like crystals also was decreased. As Pal with dry grinding treatment of 2 times, the great enhancement in specific surface area of 153 to 229 m^2/g, micropore area of 28 to 103 m^2/g, micropore volume of 0.012 to 0.047 cm^3/g was observed. In addition, with the increase of grinding times, the continuous shear stress and looping stress acting on the rod-shaped crystal of Pal increased, resulting in the fracture of rod-shaped crystal. As a result, the inherent aspect ratio of the nanofibers becomes shorter. Moreover, this result also confirmed that the appropriate dry grinding treatment had little effect on the total pore volume and external surface area, but was conducive to the production of mesopores and micropores, which had a positive effect on improving the adsorption capacity of Pal.

From these studies, it was found that dry grinding increases friction between clay particles mainly by providing mechanical force. To a certain extent, a strong mechanical force acts on the rod crystal beam of Pal, which can achieve the dissociation of the rod crystal aggregate of Pal, thereby improving the dispersion of the nanostructure for Pal. However, the single mechanical force on the dissociation degree of Pal rod crystal bundles is very limited, and the repeated dissociation of the rod bundles will reduce the aspect ratio of rod crystals and damage the rod structure, even lead to the amorphous of rod crystals. As a result, in order to maintain the aspect ratio of rod crystal, Xu et al. introduced high-pressure homogenization technology into the dissociation of Pal [17]. The Pal was homogenized with a highpressure homogenizer at different pressure (0, 10, 30, 50, 70 and 90 MPa). As shown in Fig. 2, it was clearly observed that the natural Pal is composed of many large crystal bundles and few single needle-like crystals (Fig. 2a). After homogenized at 10 MPa, the size of Pal agglomerates and the stacking degree of the crystal bundles evidently decreased. The Pal crystal bundles were further disaggregated with increasing the pressure to 30 and 50 MPa, and the length of Pal fibers is about 1 ìm (Fig. 2(c,d)). In addition, the specific surface area (from 192 m^2/g to 246 m^2/g), micropore surface area (from 72 m^2/g to110 m^2/g) and micropore volume (from 0.033 cm^3/g to 0.051 cm^3/g) of Pal were clearly enhanced after homogenization at 50 MPa. After homogenized at 70 and 90 MPa, single needle-like crystals with the lengths below 0.5 ìm appeared (Fig. 2(e, f)). At the same time, the specific surface area of the samples dropped to 238 and 237 m^2/g, respectively. This change may be related to the fracture of rod crystal and the destruction of pore structure with further increasing the shear and impact forces. These results indicated that the crystal bundles of Pal can

be effectively disaggregated while maintaining the aspect ratio of the fibrous crystals, and the high specific surface area of Pal was obtained by controlling the homogenizing pressure.

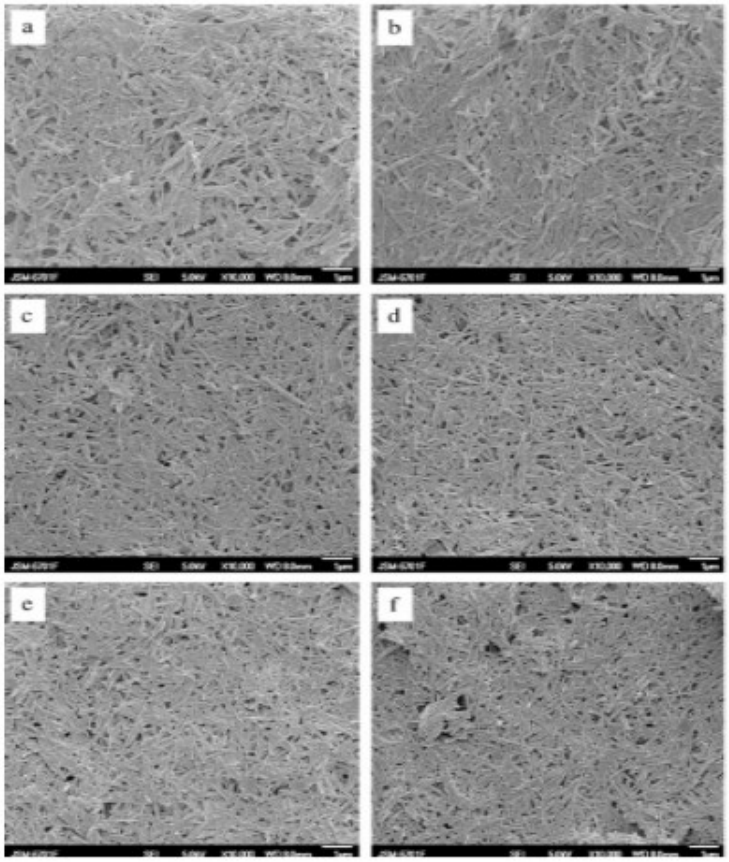

Fig. 2. FESEM images of homogenized Pal at (a) 0 MPa, (b) 10 MPa, (c) 30 MPa, (d) 50 MPa, (e) 70 MPa, and (f) 90 MPa [17].

On this basis, Xu et al. proposed a simple method combining extrusion with high-pressure homogenization technology [18]. The effects of extrusion times on the disaggregation degree of crystal bundles and microstructure were investigated at 30 MPa. However, there still have many crystal bundles with a large size in the Pal extruded only for three times without homogenization, and the specific surface area of this sample increased from 175 m^2/g to 192 m^2/g. After Pal was extruded for three times and homogenized at 30 MPa, the crystal bundles were perfectly disaggregated without disrupting the rod-like single crystals. Compared with natural Pal, the specific surface area, micropore surface area, and micropore volume of the corresponding sample increased from 175 m^2/g, 31 m^2/g, and 0.013 cm^3/g to 241 m^2/g, 103 m^2/g, and 0.048 cm^3/g, respectively. The results indicated that the further homogenization process after extrusion process played an extremely important role in disaggregating crystal bundles of Pal.

In addition to adding high pressure homogenization in the extrusion process, Chen et al. simply added the freezing process to the traditional extrusion process [19]. During the freezing process, there are much interstitial space filled by water between agglomerated crystal bundles. When water is converted to ice, the volume may expand. With the increase of the ice volume, the tightly bonded pall aggregates can be decomposed into weakly bound bundles, thus reducing the damage to the rod-shaped crystals of Pal compared with the direct extrusion treatment.

In the following work, Xu et al. systematically investigated the synergistic effect of freezing, extrusion and high-pressure homogenization on the dissociation of Pal [20]. Natural Pal was extruded with a three-roller machine for two times, and subsequently frozen at -18°C for various time (0, 4, 8, 16, and 24 h). The Pal was dispersed in water with 7 wt% of solid/liquid ratio, and stirred to form a homogeneous suspension. The obtained suspension was then homogenized at 10 MPa with the high-pressure homogenizer. The results showed that the Pal without freezing still displays many crystal bundles, but no large agglomerates. When Pal was frozen at -18°C for 4 and 8 h followed by homogenized at 10 MPa, a lot of single rods and small crystal bundles can be found. Whereas, the sample frozen for 8 h contains more small crystal bundles than the sample frozen for 4 h. Meanwhile, the specific surface area and micropore volume of the frozen Pal was increased by 45% and 170%, respectively. With the increase of freezing time, the dispersion of Pal rod crystals became worse, and larger diameter crystal bundles appear in the samples frozen for 16 and 24 h. Therefore, it is very important to choose the proper freezing time in the process of dissociation of Pal by freezing method.

As a consequently, the combination of extrusion, high-pressure homogenization and freezing methods are better than the use of single mechanical force to dissociate the rod crystals of the Pal. In addition, some scholars have developed ion irradiation to dissociate the rod crystals of Pal [21, 22]. When Pal rods are bombarded by a high-density ion beam, the stress caused by the inhomogeneous distribution of heat along the Pal axis leads to bending, elongation, shrinking, and cross-linking of the rods, thus forming the interconnected network structure. Although the dispersity of Pal rods was improved, the surface properties of Pal were also changed by irradiation treatment. However, the equipment required to produce radiation is expensive and requires a large amount of heat energy. Therefore, ion-irradiation treatment is difficult to be popularized in practical application compared with dry grinding, high-pressure homogenization and freezing technology.

As mentioned above, no matter which method is used to purify and dissociate the rod crystal of Pal, the ultimate goal is to obtain Pal with lager specific surface area and highly dispersed nanorod structure. Based on this point, our group developed a simple wet milling process to achieve the dual effect of purification and dissociation of Pal [23]. In this work, the effect of ball-to-powder weight ratio (1:3, 1:2, 1:1 and 2:1) on the crystal composition, microscopic morphology and pore structure of Pal was systematically studied by using the conventional wet ball milling process. The results show the quartz can be effectively separated from Pal through low-speed centrifugal

treatment in aqueous solutions, while the strength of ball milling has a significant influence on disaggregation degree of the crystal bundles, as shown in Fig. 3.

It can be clearly seen from Fig. 3 (a, b) that rod crystals are rarely observed in the raw Pal. After wet ball milling (1:3), the crystal bundles were partially dissociated and became fluffy. When the ratio was adjusted to 1:2, the dissociation effect of the partial rod crystals was further increased. In addition, the gaps among the rod crystals have been significantly increased, as compared with those in raw Pal. With further increase in the ball-to-powder weight ratio (1:1), the number of some shorter rod crystals is relatively increased, which indicated that although the ball milling force can partially dissociate the rod crystal bundles. However, the sample exhibited aggregation again (2:1). Furthermore, some rod-shaped crystals are seriously damaged, due mainly to the action of the excessive mechanical force. Therefore, the mechanical force should be appropriate in the wet ball milling.

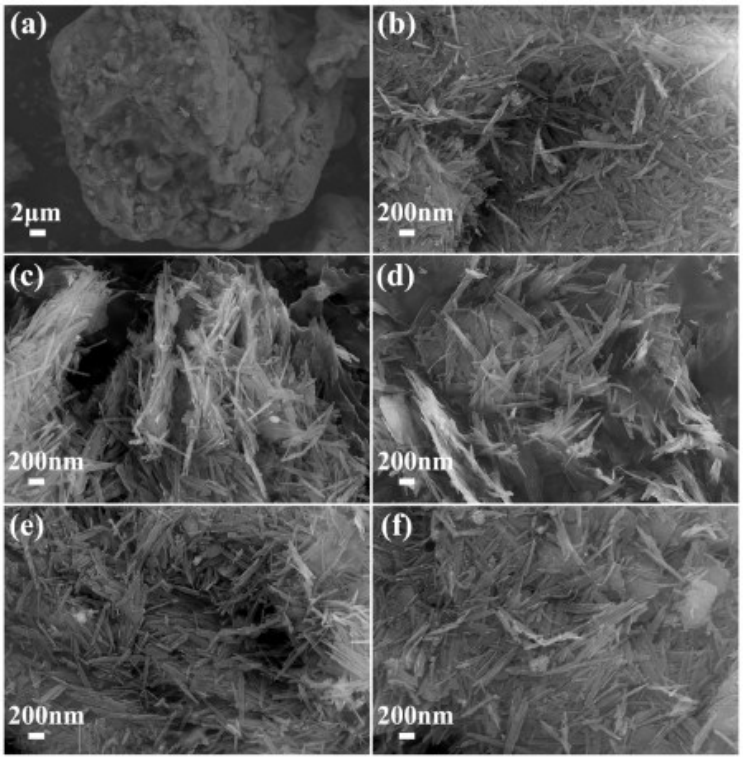

Fig. 3. FESEM images of the treated palygorskites with the different ball-to-powder weight ratio: raw palygorskite (a, b), (c) 1:3, (d) 1:2, (e) 1:1 and (f) 2:1 [23].

3.2. Modification of palygorskite

Various physical and chemical methods have been applied to modify Pal. Thermal activation is a commonly used physical method, while chemical methods include acid modification, alkali modification, organic modification and hydrothermal modification.

3.2.1Thermal activation

There are four types of water in Pal: surface absorbed water, zeolitic water in the channels, crystallized water and structural water. TGA (theromgravimetric analysis) results of Pal clay verified that the absorbed water and zeolitic water could be removed below 200!, while crystallized water was gradually released from 250! to 450! and the structural water was eliminated at e"450! [24-26].

Fig. 4 shows TGA and DTGA curves of the Pal with content of magnesium [27]. The weight loss between 30! and 160! is about 5.26%, corresponding to the removal of bound water on the surface and a portion of the zeolitic water located inside the channels, bringing of the mass loss. Between 160! and 280!, the weight loss of about 2.19% corresponds to the complete removal of zeolitic water. When the temperature is raised to 550!, the crystal water coordinated with cations on octahedral tablets disappears gradually, resulting in a weight loss of 3.7%. In this temperature range, the internal structure of Pal is rearranged, due to the removal of the water at different states, but the fibrous structure still remains unchanged. The fourth weight loss (14.7% is caused by the dehydrolyzation of Mg-OH in Pal and the decomposition of carbonate into CO_2. At 800!, Pal is completely amorphized. In other words, the crystal structure of palygorskite is absolutely destroyed, while iron oxide and quartz are present. Moreover, the density of the material is increased from 2.574 g/cm^3 to 3.038 g/cm^3 at 1000!, suggesting that the Pal is sintered at the high temperature.

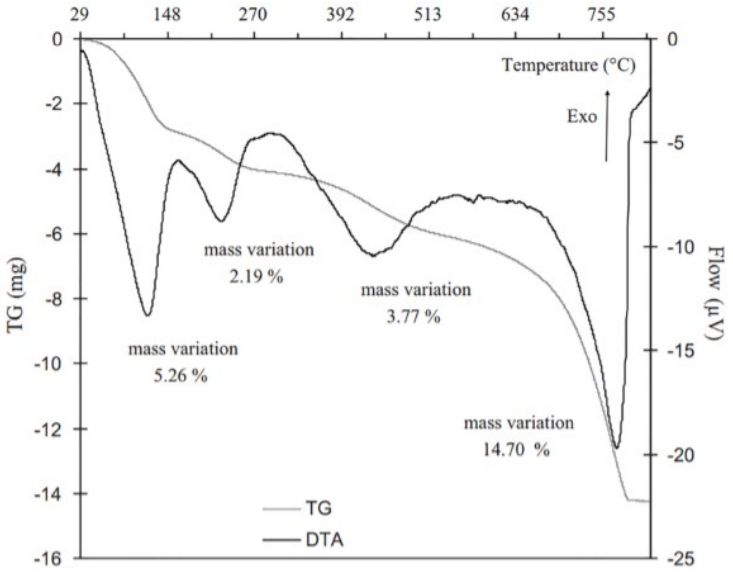

Fig. 4. TGA and DTGA curves of the palygorskite with high magnesium substitution [27].

Thermal analysis has been used to characterize purified Pal by Chen et al. [28]. It is found that the intensity of the characteristic diffraction of Pal was reduced, after calcining at temperatures of above 300!. In fact, the clay started to show structural contortions, while the specific surface area began to decline. After calcining at 600!, palygorskite

particles were still in rod shape, implying that the crystal structure had not been completely destroyed. Above 800!, the diffraction peaks of Pal completely absent, i.e., the crystal structure collapsed and the amorphization process started accordingly. Meanwhile, cristobalite was present as a new phase. At 1000!, the nano-gap between the particles of Pal disappeared and the material was sintered to a certain degree. This observation is similar results discussed above [27].

In summary, a proper thermal activation could loosen the channels of Pal, so that the void volume and specific surface area are increased. As a result, more surface active sites will be available for absorption. However, too high temperature resulted in crystal structure collapse of palygorskite, thus leading to a decrease in both the void volume and specific surface area, which in turn weakens the sorption behavior of the clays [29]. Moreover, as the calcination temperature is higher than 500!, the fibrous crystal is melted and new crystalline phases are present. Therefore, the calcination temperature to remove water molecuels in palygorskite should be < 500! [30, 31].

3.2.2 Acid and alkali activation

The acidification is mainly to remove the non-adsorptive active impurities (such as carbonates) which are attached to the channels, so that the channels are loosened. In addition, H^+ with a smaller radius in acid solution can displace such ions as K^+, Na^+, Ca^{2+}, Mg^{2+}, which results in an increase in the volume and number of the channel and thus enhancement of the ion exchange capacity.

Boudriche et al. evaluated the effect of concentration of hydrochloric acid (HCl) of the properties of Pal [32]. Fig. 5 shows XRD patterns of the caly before and after treatment with HCl at different concentrations. It was found that the peak intensities of dolomite and calcite were decreased gradually with increasing concentration of HCl. After treating with 0.5 M HCl, the XRD pattern was almost unchanged. However, the specific surface area was increased from 125.1 m^2/g to 273.5 m^2/g after the HCl treatment. As the concentration of HCl was increased to 1 mol/L, the diffraction peaks of calcite ($CaCO_3$) and dolomite ($CaMg(CO_3)_2$) disappeared. Decarbonization brought out an increase in both the volume of pores and the apparent density of the sample, resulting in a specific surface area of 336.6 m^2/g. In this case, the diffraction peaks of Pal remained unchanged. If the concentration of HCl was increased to 3 mol/L, the peaks of Pal were widened, indicating the decrease in the degree of crystallization. Meanwhile, the specific surface area was increased to 399.0 m^2/g, due to the decomposition of the large amount of carbonate, the dissolution of some octahedral sheets and the exchangeable cations, which all produce new surfaces in the Pal. After the sample was treated with 5 mol/L HCl, the diffraction pattern of the Pal was characterized by a broadened and widened band between 15^o and 35^o (2è). This was attributed to the dissolution of the octahedral sheet in Pal and the formation of amorphous silica. At the same time, the microporous volume was decreased, while the deposition of insoluble acid medium led to the plugging of the active sites, so that the specific surface area of Pal was decreased to 315.2 m^2/g.

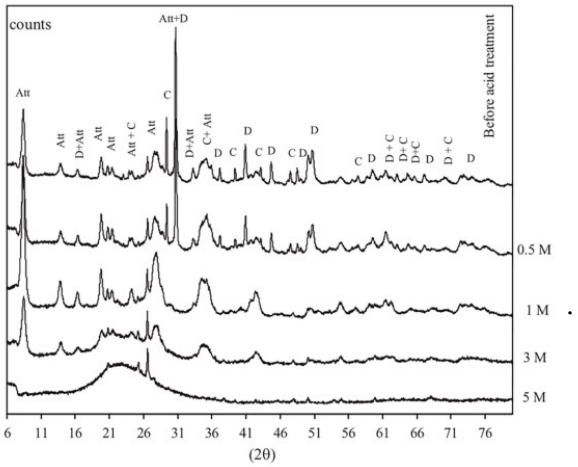

Fig. 5. XRD patterns of the palygorskite before and after acid activation at different concentrations of HCl (Att = palygorskite, D = dolomite, C = calcite) [32].

Wang et al. used a simple one-step hydrothermal acid leaching process to efficiently convert natural Pal to porous silica nanorods with a high SiO_2 content and decent length of nanorods [33]. In this study, natural Pal (4g) was dispersed in 60 ml HCl aqueous solutions with concentrations of 0.1, 0.5, 1.0, 1.5 and 2.0 mol/L, respectively, to form a uniform aqueous suspension. The reaction was carried out at 140! for 6 h. For a comparison, natural Pal was also treated with different concentrations of HCl solution at 80 ! for 6 h under re-flux and agitation. As shown in Fig. 5a, the rods are aggregated together in natural Pal. After being treated with 0.1 mol/L HCl aqueous solution under hydrothermal condition, the crystal bundles of Pal were decomposed into smaller crystal bundles or single nanorods, and the length of the crystal has not change compared with the untreated Pal (Fig. 5b). With increasing the concentration of acid solution, the dispersibility of the rod crystals was further improved because the carbonate or organic impurities present in rods may be decomposed by the acid treatment under hydrothermal condition(Fig. 5c–f). In addition, It is interesting that the shape and original length of Pal rods still remain well even after treatment with 2.0 mol/L HCl solution under hydrothermal reaction condition (Fig. 5f), while the rod structure of Pal was broken seriously and the length of rod was shortened greatly after the normal acid treatment process at atmospheric pressure (Fig. 5g). As comparison, the raw Pal was also treated with 4.0-8.0 mol/L of HCl solution by a reflux process at 80 °C. It is obvious that the longer Pal rod crystal becomes shorter and the rod crystals still aggregate together even after treatment with 8.0 mol/L aqueous HCl solution (Fig. 5i). The surface of the rod-shaped crystal becomes coarse and many particles appeared around the rods. In other word, the acid leaching with high concentration acid solution leads to the serious fracture of Pal rod crystal and even the disappearance of rod crystal. This is basically consistent with the above research. As a result, the shape of Pal rods still remains better and the silica nanorods with the same length as original Pal rods can be obtained after treatment with 2.0 mol/L HCl solution under hydrothermal condition compared with the conventional acid leaching method.

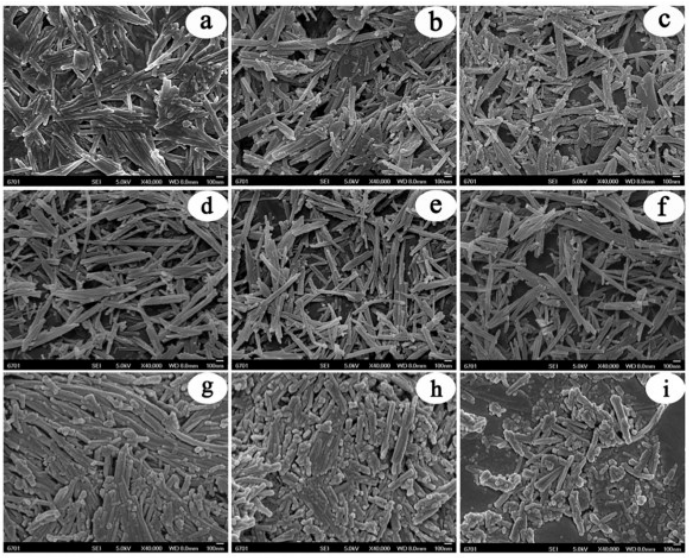

Fig. 6. SEM images of the raw palygorskite (a) and the acid-leached palygorskite with 0.1 (b), 0.5 (c), 1.0 (d), 1.5 (e), 2.0 (f) mol/L of HCl solution under hydrothermal reaction condition and the acid leached palygorskite with 2.0 (g), 4.0 (h), 8.0 (i) mol/L of HCl solution under normal atmospheric condition at 80°C [33].

In conclusion, at low concentrations of acid, the specific surface area of Pal increases with increasing acid concentration and acidification time. As the concentration of acid is sufficiently high, numerous Si-OH groups will be produced on the surface of Pal, i.e., the number of active sites is increased, so that the adsorption capacity of Pal is enhanced. However, excessive content of acid will cause damage of the octahedral and tetrahedral structures in Pal, which may lead to the long rod crystal can be broken as shorter rods or particles. As a consequence, the specific surface area will be decreased and amorphous silica is formed to adhere to clay surface, weakening the adsorption and decolorization capabilities [34-36]. Therefore, in the study of acid treatment of Pal, it is very critical to maintain the rod structure of Pal as much as possible by controlling the acid concentration and acid leaching method.

Alkali treatment can activate the Si-O-M (M is metal ion) group and Si-O-Si group on the surface of Pal into Si-O- groups, thus increasing the surface negative potential and the number of active adsorption site. For example, Wang et al. modified Pal with NaOH solution, leading to alkali-activated Pal whose adsorption efficiency to methylene was greatly increased [37]. The principle reactions are as follows:

$$\text{Si-O-Si} + \text{OH-} = \text{Si-O-}, \quad (1)$$

$$\text{Si-O-M} + \text{OH-} = \text{Si-O-}. \quad (2)$$

3.3 Organic modification

The heat treatment of palygorskite mainly results in the maximization of surface area by removing the four states of water, while the acid/alkali treatment increases the

number of acid-base active sites by breaking the covalent bonds on the surface of Pal. Although the change of the structural pore and surface acid-base properties can improve the adsorption capacity of Pal to a certain extent, the method is only to touch the structure of the Pal itself. In order to further enhance the adsorption property of Pal, it could be combined with some organic materials with special properties. The most frequently used modification methods with organic materials include surfactant modification, coupling agent modification and chemical grafting modification.

3.4 Surfactant modification

On one hand, surfactant modification is to make use of the cation exchange behavior of Pal, i.e., organic cations with long carbon chains enter the inter-layer spacing of Pal to replace inorganic cations, such as Mg^{2+}, Al^{3+} and Fe^{3+}, so that the layer spacing is increased [38, 39]. On the other hand, by utilizing the negative charge on the surface of Pal, the positive charge group in the surfactant is adsorbed on the negative charge sites. Therefore, the hydrophobicity and surface charge of the rod crystal are altered [40, 41].

Common cationic surfactants include OTMAC, OTAB, CTAB and so on. Huang et al. applied OTMAC to modify Pal. The OTMAC-ATP adsorbent was used to adsorb tannin from flavonoids [42]. Through the hydrogen bond and electrostatic interaction, the introduction of OTMAC increased the hydrophobic behavior of Pal, so that selective adsorption of tannin was enhanced. Lei et al. treated Pal clay with CTAB of different concentrations [43]. According to dielectric properties, it was found that CTAB had a significant effect on electrorheological characteristics. Besides, anionic surfactants have also been employed to modify Pal. In this case, by attaching metal oxides on the surface of Pal or protonating palygorskite under acidic conditions, so that the clay surface can be positively charged, thus allowing anionic surfactants to modify Pal. Xu et al. used sodium oleate as anionic surface active agent to organically modify palygorskite clay [44]. It was observed that the positively charged species on the surface of palygorskite combined with oleate ions. As a result, due to the attachment of the long alkyl chains, the hydrophobicity of the Pal surface was increased, thus leading to a decrease in the shear viscosity of the suspensions. Because it is necessary to coat metallic oxides on the surface of Pal, this organic modification process consists of two steps, making the experimental process more complex than the cationic process, so that there are relatively fewer reports on the modification of Pal with anionic surfactants in the open literature. Nevertheless, it is still deserved to be further studied from both the academic and practical views.

3.5 Silane coupling agent modification

Silane coupling agent modification is to attach silicon hydroxyl group on the surface of Pal. Silane coupling agent is an organosilicon compound, which comprises of two chemical groups, i.e., reaction group and silicon hydroxyl group. Reaction groups include methoxy group, ethoxy group, amino group, epoxy group, double bond group and so on. Silicon hydroxyl groups are derived from the hydrolysis of silane coupling agent,

which have a condensation reaction with the hydroxyl groups on the surface of Pal, thus forming chemical bonds.

Xue et al. proposed a mechanism to describe the reaction for the coupling process of APTES (aminoproplytriethoxysilane) [45]. With the presence of water, APTES reacted with the surface hydroxyl group of Pal. Firstly, APTES was hydrolyzed, followed by the reaction between silanol intermediates (Si-OH) and the hydroxyl group on the surface of Pal. Finally, self-polymerization occurred with the silanol intermediates.

3.6 Chemical graft modification

Chemical graft modification is to attract polymers with different functional groups onto the surface of Pal through chemical bonds, thus increasing the number of active groups. As a consequence, the complexation capability of Pal is increased dramatically. For example, Peng et al introduced chitosan to the surface of Pal by using a surface grafting technique [46]. The authors found that that the adsorption capacity of the chitosan-modified Pal to 3Rs was obviously higher than that of the non-modified Pal. Liu and Guo brought amidogen of polyacrylamide to palygorskite surface successfully [47]. Owing to the chelation of amidogen with Hg(II) ion, monoamido- or diamido-Hg structures could be readily formed. Therefore, the selective adsorption of Hg(II) was significantly improved [48].

3.7 Potential applications

3.7.1 Applications as adsorption materials

Due to the negative charges on the surface, natural Pal clay is an ideal adsorbent. However, natural Pal contains various impurities, so that it is usually needed to go through modification to have stronger adsorption capabilities, as discussed above. Chen et al. studied the effects of heat treatment on the acid-alkali properties and adsorption capacities of Pal by adopting the alkaline gas NH_3 and acid gas SO_2 as criteria [49]. The authors believed that there are two mechanisms for the adsorption of both NH_3 and SO_2: (i) surface physical adsorption and (ii) chemical adsorption at the acid-alkali sites. Between 50! and 150!, the adsorption capacity of Pal was increased from 1594 ìmol/g to 1661 ìmol/g and 415 ìmol/g to 509 ìmol/g for NH_3 and SO_2, respectively. This was attributed to the absence of the zeolite water in the pores of Pal, as a result of the calcination below 200!, which increased the specific surface area of Pal. Therefore, the pores could accommodate more NH_3 and SO_2 molecules. Furthermore, the loss of a large number of hydroxyl groups in Pal led to the loss of the acid adsorption centers. As a consequence, the capacity of Pal adsorb NH_3 was about 3 times of that of SO_2. Above 150!, the adsorption capacity to NH_3 was gradually decreased to 335 ìmol/g. Although the specific surface area of the Pal reached the maximum after calcining at 200!, the amount of NH_3 adsorbed by Pal was decreased dramatically. It was believed that the pore folding in the Pal calcined at above 200! blocked the NH_3 molecules to enter the inner surface of Pal. After calcining at higher temperatures, the coordination water and

structural water were removed, thus increasing the pore folding and causing hydroxyl dehydration, so that the number of the surface acidic active site was reduced, resulting in a sharp decrease in the adsorption capacity to alkaline NH_3. However, the adsorption capacity of SO_2 was decreased to 268 ìmol/g after calcining at 250!, which was resulted from the fact that SO_2 could not enter the folding channels. As the calcination temperature was further increased, the dehydration of surface hydroxyl groups occurred, thus leading to an increase in the alkali adsorption center, so that the adsorption capacity to SO_2 was increased to 362 ìmol/g at calcining 300!. For the sample calcined at 550!, the channels were completely collapsed and amorphization was started. Once the amorphization began, both the acid and base active sites on the surface were started to lose. In this case, the two gas molecules were only adsorbed thorugh external adsorption.

Srasra and Frini-Srasra treated palygorskite clay with HCl in order to enhance the adsorption capability to Cd(II) in water [50]. After the treatment with HCl at the concentration of 2 mol/L, the specific surface area of Pal was increased from 59.7 m^2/g to 437 m^2/g, due to the dissolution of the octahedral sheet and the creation of mesoporosity. Accordingly, the adsorption capacity to Cd(II) was largely enhanced. The maximum adsorption capacities to Cd(II) in aqueous solution were 118 mg/g and 90 mg/g for acid treated and natural Pals, respectively.

Chen et al. studied the effect of treatment with HCl at different concentrations [51]. It was revealed that the specific surface area of Pal was increased gradually with increasing concentration of HCl. The specific surface area reached the maximum level of 267.5 m^2/g at 12 mol/L HCl, while the adsorption capacity to Cu(II) also reached the maximum value of 32.24 mg/g. IR spectrum showed that the absorption bands of carbonate minerals at 1437, 881 and 728 cm^{-1} disappeared after acid treatment and a new absorption band at 3730 cm^{-1} appeared, due to the OH stretching vibration of silica group on the surface of Pal. In addition, as the concentration of HCl was increased, the strength of the OH adsorption band of silica group was increased gradually, indicating that the number of silicon-groups on the surface of Pal was increases. The main mechanism of Cu(II) adsorption by the acid activated Pal is the complexation of surface silicon group with Cu(II), according to the kinetic simulation. The reaction process is as followsÿ

$$Si\text{-}OH + Cu^{2+} = Si\text{-}OCu^{+} + H^{+}, \quad (3)$$

$$2Si\text{-}OH + Cu^{2+} = (Si\text{-}O)_2Cu + 2H^{+}, \quad (4)$$

$$Si\text{-}OH + Cu^{2+} + H_2O = Si\text{-}OCuOH + 2H^{+}, \quad (5)$$

$$Si\text{-}OH + 2Cu^{2+} + 2H_2O = Si\text{-}OCu_2(OH)_2 + 3H^{+}. \quad (6)$$

Although thermal activation and acid activation could be used to enhance the heavy metal ion adsorption capacity of Pal owing to the increase in specific surface area and the number of adsorption sites, adsorption through pores and surface complexation is limited. Therefore, graft modification is more effective in increasing ion adsorption capability of Pal.

Wang et al. prepared the floatable porous sodium alginate based Pal foam by using freeze-drying and post-cross-linking methods [52]. They examined the effect of Pal/SA ratio on the adsorption properties of copper ions and isolated ions. As the loading capacity reached to 20 wt% (SP-0.25), the adsorption capacity of, Cu(II) and Cd(II) were 109.3 mg/g and 147.2 mg/g, respectively, of which the adsorption capacity hasn't changed much compared with pure sodium alginate foam (SP-0). When the loading capacity was 33.3%, the adsorption capacity of SP-0.5 decreased and the content of COO- in SA reduced. The adsorption capacity was derived from Langmuir isotherm model, and its maximum adsorption capacity was: Cu(II) 119.0 mg/g and Cd(II) 160.0 mg/g respectively which showed a high inosculation with the actual adsorption capacity of composites. Therefore, the adsorption process was in good agreement with the pseudo-second-order kinetic model, and the rate limiting step of adsorption was an chemical interaction process. In addition, SA was utilized to immobilize Pal and to minimize its loss, and Pal was uniformly dispersed in sodium alginate polymer matrix, which was beneficial to improve the mechanical properties of the polymer. In the adsorption test, the low density of porous foam made them float and was easy to recycle. These adsorbents have strong chemical stability and high recycling possibility owing to their floatability in water solution.

Mao et al. synthetized Pal hydrogel adsorbent, with Pal, sodium alginate and sodium polyacrylate as the raw materials [53]. Due to the presence of carboxyl groups in three-dimensional gel network, the adsorption capacities of the hydrogel with 10% Pal were 272.8 mg/g for Cu(II) and 391.7 mg/g for Pb(II).

Cui et al. prepared polyaniline/palygorskite (PANI/Pal) adsorbents through chemical oxidation, as the adsorbents for Hg(II) [54]. The fiber structure of Pal prevented the aggregation of PANI, enlarged the specific area and enhanced adsorption capacity of composites. The studies of kinetics confirmed that the Hg(II) adsorption by PANI/ATP followed the pseudo-second-order kinetic model, implying that the adsorption of Hg(II) was predominantly a chemical process. The coordination mechanism of the amino groups grafted on the surface of Pal and Hg(II) was a clear evidence, which was in a good agreement with the above results.

Liu et al. grafted carboxymethyl cellulose-g-polyacrylic acid onto the surface of Pal in order to improve its adsorption capacity to Pb(II) in aqueous solution [55]. It was found that the surface electrostatic force, cation exchange capacity and coordination force were all essential factors that affected the Pb(II) adsorption behavior of the composite adsorbents. IR spectra before and after adsorption showed that -COOH, -COO, and -NH- groups were involved in the adsorption process. Furthermore, R^2 obtained by linear fitting the pseudo-second-order model parameters was better than that based on the pseudo-first-order model. Therefore, complexation might be the main adsorption mechanism of the composites to Pb(II). Specifically, the adsorption capacities were 920.3, 906.4, 856.8, 791.7 and 737.2 mg/g, for the APT contents of 5, 10, 20, 25 and 30 wt.%, respectively. It was revealed that the adsorption capacity was decreased with increasing content of Pal, because Pal participated in the polymerization process,

by acting as the crosslinking points in the network. As a result, the cross-linking strength was increased, so that the numbers of the carboxyl group and the active point were reduced. In other words, the carboxyl group is the main functional group in the CMC-g-PAA/APT hydrogel composites to adsorb Pb(II).

Chen and Wang prepared poly(acrylamide)/palygorskite composite adsorbents by using polyacrylamide and Pal as the raw materials [56]. It was approved that there were three types of adsorption sites in the composite, where were $-COO^-$, $-COO-Na^+$ and $-CONH_2$. After adsorption of Cu(II), the intensities of the IR characteristic peaks of the three functional groups were reduced obviously, indicating that electrostatic attraction (physical adsorption), ion exchange and chelating adsorption were involved in the adsorption process. In addition, due to the complete saponification, there was small amount of $-COO^-$ and $-COO-Na^+$ in the composites. Therefore, it can be considered that $-COO-Na^+$ and $-CONH_2$ were two dominating groups. The EA value exceeded the corresponding range of ion-exchange, indicating that the adsorption mechanism followed the chelation model. During the adsorption process, it was noticed that the adsorption capacity of the composites was increased rapidly at the initial stage of adsorption. As the contact time was prolonged, the adsorption capacity was continuously increased at a relatively slow rate. 90% of the adsorption was completed in the first 10 min, until the equilibrium point was reached after 90 min. Since then, there was only little further increase. The maximum adsorption capacity of the non-modified Pal was only 32 mg/g in 180 min.

Pal is also able to adsorb dye molecules in water. Chen et al. reported the effect of calcination temperature on adsorption capacity of palygorskite for methylene blue (MB) [7]. The authors found that the specific surface area of palygorskite started to decrease, but the adsorption capacity reached the maximum at 700!. Moreover, the cation exchange capacity of the sample, the fraction of mesopores and distribution of pore size were all improved by the calcination treatment. The enhancement in cation exchange capacity was the main reason for the enhanced adsorption performance.

Wang et al. prepared Pal adsorbents activated in alkali solution [37]. It was found that the specific surface area of palygorskite reached almost zero after activation in 5 mol/L of NaOH solution. The adsorbents, however, still exhibited excellent adsorption function for MB, due to the strong hydrogen-bonding interaction, electrostatic attraction and chemical association.

Tian et al. modified natural Pal with sodium sulfide solution at different concentrations [57]. The synergetic effects of hydrothermal process and sodium sulphide on structure, physico-chemical features and methylene blue adsorption properties were studied. Sodium sulfide, as a strong base-weak salt, which is hydrolyzed slowly in water to produce Na^+, HS^- and OH^- groups, thus having alkaline characteristics. OH^- attack can destroy Si-O-Si and Si-O-M bonds and bring about partial evolution of the crystal structure. The broken Si-O- band could be in the form of -Si-O (Na), which caused the crystal structure of Pal to evolve into silicate with high adsorption activity, resulting in

the increase of negative potential on the surface of Pal and thus displaying excellent adsorption capacity to cationic dyes. With the effects of electrostatic interaction, pore adsorption and chemical association of the -Si-O- groups, the modified Pal was able to remove MB thoroughly in the solution with an initial concentration of 200 mg/L. As the concentration of sodium sulfide climbed to 0.048 mol/L, the adsorption capacity was increased from 129.71 mg/g to 187.56 mg/g, indicating that it could be a strong absorbent for dye waste water purification.

3.7.2 Factors affecting adsorption capacity of palygorskite-based adsorbents

The adsorption capacity of an absorbent is closely related to a number of factors, such as the quantity of the adsorbent used, the time of adsorption reaction, the initial concentrations of the metal ions or organic dyes and the initial pH value of the solution. Obviously, a high content of adsorbent, a long contact time and a high initial concentration of the metal ions or organic dyes would make more adsorption molecules attach to the surface of the adsorbent. Also, at given conditions, more adsorption activity site means high adsorption capacity. However, the adsorption rate always reaches saturation and adsorption reaction approached equilibrium state. The effect of pH value of the initial solution on the adsorption activity of Pal-based adsorbents is discussed as an example. At low pH values, H^+ ion in the solution has a competitive adsorption with the pollutants with positive charge in water, suppressing the adsorption capacities for the heavy metal ions and cationic dyes [58-60]. Usually, at high concentrations of H^+ (low pH values), the positive charges on the surface of adsorbents have an electrostatic attraction with the anionic dyes, thus leading to an increase in the anion removal rate. At high pH values, adsorbents remove the heavy metal ions and cationic dyes in water through ion exchange, electrostatic interaction and complexation. Under an alkaline condition, Si-O- bond on the surface of the adsorbent generates electrostatic repulsion with the anionic dyes, resulting in a drop in the adsorption rate [61, 62]. The principle is shown in Fig. 7.

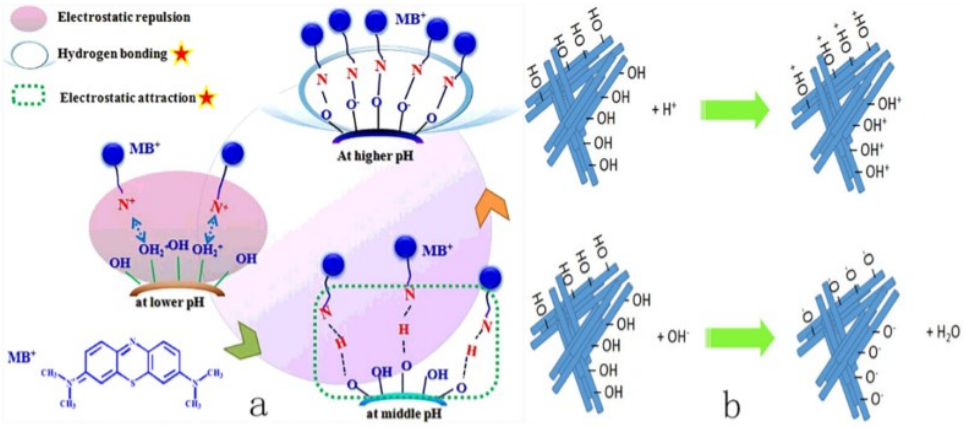

Fig. 7. (a) Adsorption representation of MB onto palygorskite at different pH values [57]. (b) Schematic representation of charges generated on clay mineral surfaces at different pH values [61].

3.8 Applications as composite photocatalytic materials

To develop efficient, green and low-cost strategies to deal with pollutants, Pal has used as the support of photocatalysts, due to its strong adsorption performance and large specific surface area.

Papoulis et al. prepared Pal-TiO_2 nanocomposites by deposition of anatase form of TiO_2 on the Pal surfaces using a sol-gel method with titanium isopropoxide as a precursor under hydrothermal treatment at 180°C [63]. It was observed that the commercial titania P25 showed no absorption in visible light region. In contrast, the prepared TiO_2 has good dispersibility on Pal and the prepared Pal/TiO_2 samples showed gray color and absorption in visible light region. In addition, in the process of NO_x gas decomposition, it was found that the catalytic activity of the composite with the mass ratio of Pal to TiO_2 of 3:7 was 2.61 times higher than that of commercial titanium dioxide (P25) under visible light irradiation (ëÿ510 nm) and 1.15 times higher under ultraviolet light irradiation (ëÿ290 nm) [64].

Huo et al. used copper oxalate as a precursor and deposited CuO nanoparticles on the surface of silicate nanofibers (Pal) by precipitation to prepare Pal/CuO nanocomposites [65]. The photocatalytic degradation of methyl orange under the irradiation of ultraviolet light was investigated. X-ray diffraction and transmission electron microscopy characterization showed that the surface of Pal fiber with a diameter of 20-30 nm and a length of 400-500 nm was uniformly modified with CuO nanoparticles with an average particle size of 16 nm. The results showed that the presence of Pal may enhance the surface adsorption of the composite photocatalyst at the interface, coupled with efficient electron-hole separation, the photocatalytic activity of the composite material is significantly higher than that of pure CuO.

Liu et al. prepared BiOBr/Pal photocatalyst for the first time by hydrothermal method [66]. The photocatalytic degradation behavior of methyl orange was evaluated under visible light irradiation. The results revealed that BiOBr/Pal composites had strong photoabsorption in the visible light region. All BiOBr/Pal composites possessed higher photocatalytic activity than pure BiOBr. The enhanced photocatalytic performance was attributed to strong photoabsorption, the synchronous role of adsorbability and photocatalytic oxidation on BiOBr/Pal composites and the efficient separation of photogenerated electron–hole pairs.

Chen et al. modified Pal with a certain amount of CTAB for ion exchange reaction, and then prepared Pal/TiO_2 composites with different proportions by sol-gel method [67]. It was found that the photocatalytic activity of Pal/TiO_2 composite was higher than that of pure TiO_2 in the degradation experiment of methylene blue under UV irradiation because of the large specific surface area of Pal as carrier. In addition, the photocatalytic activity of Pal/TiO_2 samples increased with the increase of TiO_2 content in nanocomposites. In order to improve the light response of the composites to the visible light region, the authors introduced CdS (0.1-0.4mol/L) of different concentrations into the Pal/TiO_2 composites to prepare the Pal/TiO_2/CdS ternary photocatalyst. The results

showed that the photocatalysis efficiency of all Pal/TiO_2/CdS nanocomposites was higher than that of Pal/TiO_2 and Pal/CdS, and the photodegradation efficiency increased with the increase of CdS content. When the concentration of CdS is 0.4 mol/L, the photodegradation efficiency of Pal/TiO_2/CdS can reach 37% after 150 min Under visible light.

The excellent photocatalytic properties of Pal/TiO_2/CdS nanocomposites under visible light can be attributed to: One reason is that CdS is a narrow-band semiconductor that can be excited by visible light to produce light-induced electrons and holes. The light-induced electrons and holes can oxidize MB into its free radical cations directly or through the predominantly formed ·OH. This rapid electron transfer between CdS and TiO_2 may accelerate the oxidation of MB. Another reason is that as the carrier of CdS and TiO_2, Pal can not only prevent the agglomeration of nanoparticles, but also absorb MB molecules to gather near TiO_2 and CdS, thus accelerating the photocatalytic reaction.

Zhang et al. attached the Pal modified with CTAB to Cu/TiO_2 photocatalyst [68]. It was concluded that both the hydrophobicity and the number of the micro-mesopore in the nanocomposite were increased, resulting in an acetone degradation rate of 90.4% in 6 h.

Ma et al. adopted a precipitation method to load Ag_3PO_4 particles onto the surface of Pal, resulting in uniformly distributed spherical particles without obvious aggregation [69]. Photocatalytic properties of the Pal, Ag_3PO_4, Ag_3PO_4-Pal-Co and Ag_3PO_4-Pal-Pr composites were examined through the decolorization of Orange II under the irradiation of Xe arc lamp and sunlight. It was revealed that there was little reaction in the system of natural Pal under the irradiation of Xe arc lamp for 160 min, while Pal-supported Ag_3PO_4 can be used for degradation under sunlight irradiation. Furthermore, Ag_3PO_4-Pal-Co particles had a stronger activity than the Ag_3PO_4-Pal-Pr particles. When it was exposed to Xe arc lamp and the irradiation of sunlight, the degradation rate of the Ag_3PO_4-Pal-Co-catalyzed solution within 90 min for the Xe arc lamp and the sunlight was about 99%. This was because the Ag_3PO_4 particles had small size and were uniformly distributed on Pal.

Heterogeneous photocatalytic degradation generally occurs after the reactants are adsorbed on the surface of the catalysts, so that adsorption is actually a previous step of the subsequent photocatalytic reaction. Pal is a widely studied adsorbent for removing organic pollutants due to its nano-rod-like structure. The specific surface areas of Ag_3PO_4 and Ag_3PO_4-Pal-Co were 23.5 and 365 m^2/g, respectively. The data indicated that the loading of Ag_3PO_4 increased the specific surface area of Pal. Moreover, the content of Ag in the photocatalyst composite was decreased from 77.3 wt% in bare Ag_3PO_4 to 18.8 wt% in the Ag_3PO_4-Pal-Co composite. Both the photocatalytic activity and stability of Ag_3PO_4 were significantly improved when they were loaded on Pal.

Wang et al. reported palygorskite/CdS (Pal/CdS) nanocomposites reparaed by using a hydrothermal method, in order to study the effects of CdS content on the color degradation and photocatalytic performance of the nanocomposites [70]. The reaction

precursor solution was prepared by dissolving $CdCl_2 \cdot 2.5H_2O$ and thiourea with a certain molar ratio into 15/ mL water. After continuous stirring for 1 h, the precursor was dripped into Pal suspension. When the content of CdS was 40%, the Pal/CdS showed a wide absorption band in the range of 360 500 nm. Since blue and green are complementary colors of yellow and red, respectively, Pal/CdS and CdS (180!) showed yellow and red. Besides, the absorption edge of the composite shifted to shorter wavelength (from 538 nm to 522 nm), as compared with that of CdS (180!). Also, due to the quantum size effect, the decrease in particle size of CdS in Pal/CdS also had contribution to the increase in the band-gap energy. The sample with 40% CdS had the maximum apparent band-gap energy of 2.37 eV, thus displaying the highest photocatalytic activity under the irradiation of visible light. The photocatalytic degradation efficiencies of MV and CR were 100% and 99% respectively in 70 min. The photocatalysis mechanism of the Pal/CdS nanocomposites is schematically shown in Fig. 8. Charge separation begins in Pal/CdS, while electron-hole pairs (e^- and h^+) in CdS produce -OH radical from the dissolved O_2 and water. Then, these active species converted MB dye molecules into CO_2 and H_2O finally. Such Pal/CdS nanocomposites can be used as effective photocatalysts for degradation of organic dyes.

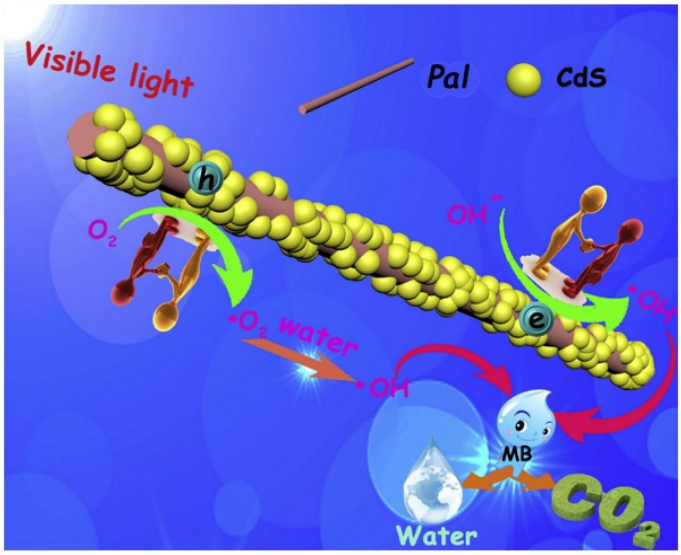

Fig. 8. Schematic presentation of the charge separation and transfer of electrons in the Pal/CdS nanocomposites under visible light illumination [70].

Li and Peng assembled the MoS_2 nanosheets with polycrystalline structure and abundant defect sites in situ on the Pal nanofibers by hydrothermal method [71]. It was found that the Pal nanofibers can prevent the aggregation of MoS_2 nanosheets, thereby providing a larger specific surface area and more reaction sites. In addition, the introduction of Pal can also improve the hydrophilicity and dispersibility of the composites in the water phase. The synergistic effect of more reaction sites in the hybrid

nanostructure and the hydrophilicity of Pal make the catalytic activity of the MoS_2/Pal composite material higher than that of pure MoS_2 synthesized by hydrothermal method. During the reduction of 4-NP, it was found that with MoS_2/Pal as the catalyst, the decolorization rate of 4-NP could reach 99.72% after 10 min.

Our groups recently reported Pal supported spherical ZnS hybrid nanocomposites, which were synthesized by using a simple hydrothermal method [72]. It has been confirmed that the introduction of Pal could effectively prevent ZnS from the free self-aggregation, thereby increasing the specific surface area of Pal/ZnS nanocomposites (from 36.33 m^2g^{-1} to 83.85 m^2g^{-1}). The prepared nanocomposites exhibited a significant enhancement in photoactivity for the degradation of Rhodamine B under simulated sunlight irradiation. Specifically, when the content of Pal was 40%, the nanocomposite showed optimal photocatalytic activity, with a degradation rate of rhodamine B of 100% in 150 min. The improved photocatalytic performance of the nanocomposites may be attributed to the fact that the incorporation of Pal not only strengthened the adsorption of Rhodamine B, but also reduced the band gap energy of the nanocomposites and the recombination rate of electrons and holes. In addition, as revealed in Fig. 9 (a), the photocurrent of the 40%-Pal/ZnS nanocomposites was higher than that of the pure ZnS. Meanwhile, the EIS spectra of 40%-Pal/ZnS in Fig. 9 (b) showed a smaller semicircle than that of pure ZnS nanoparticle. The results showed that the effective separation of photo induced carriers and the enhancement of interfacial electrons transfer efficiency also play an important role in enhancing the photocatalytic activity of the 40%-Pal/ZnS nanocomposites.

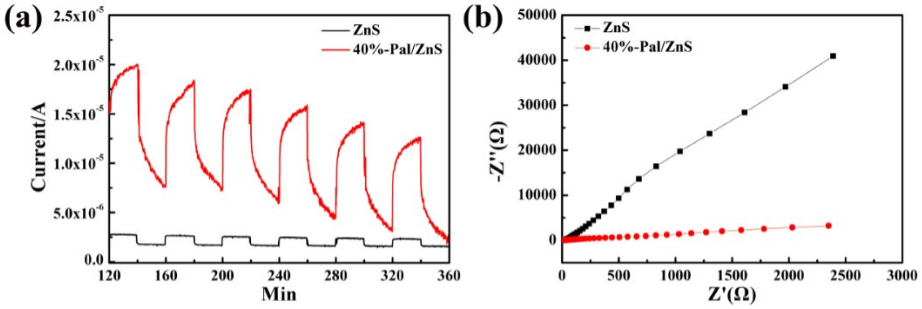

Fig. 9. (a) Transient photocurrent responses under visible light irradiation. (b) Electrochemical impedance spectroscopy (EIS) Nyquist plots of the as-synthesized catalysts in 0.5 mol/L Na_2SO_4 solution [72].

The function of Pal in the composite photocatalysts is to improve the dispersion of the active photocatalyst and increase the specific surface area and the number of adsorption sites of the composite. Moreover, the photocatalytic activity of the composites is increased due also to the fact that the pollutants to be degraded by the photocatalyst are more efficiently transported to the decomposition centers given the strong adsorption capacity of Pal [73]. However, the biggest issue now is the ambiguity of the mechanism for the interactions of Pal with the doping ions and the photocatalyst components. In addition, because of the differences in photocatalytic reaction devices used in different laboratories and the distinction among the wavelengths of light sources, irradiation

power and characteristics of the synthetic wastewaters, it should be very careful when using the conclusions reported in the open literature.

3.9 Applications as composite microwave absorption materials

Nowadays, with the development of science and technology, due to the wide application of electronic products in daily life, electromagnetic interference and radiation become extremely serious. In order to solve the impact of these electronic products on human health. In recent decades, the development of microwave absorbing materials has attracted much attention, including ferrite, magnetic alloy , carbon material and conductive polymers [74, 75]. However, nanoparticles tend to agglomerate in the synthesis process, which is a common disadvantage of nanocomposites. Therefore, in order to improve the dispersion of nanomaterials, it is very important to choose a low consumption and suitable dispersion matrix. In recent years, Pal has unique rod-shaped structure, rich pore structure, high specific surface area, non-toxic, low cost and adjustable surface chemical properties, which show excellent supporting properties in adsorption, catalyst and polymer nanocomposites. As a carrier of microwave absorbents, it has attracted extensive attention in recent years.

Our group recently reported that purified Pal was used as a carrier to enhance the microwave absorption performance of magnetic Fe_3O_4 particles [23]. The results showed that the introduction of Pal can effectively prevent the free aggregation of Fe_3O_4 nanoparticles. the dispersion of magnetic nanoparticles on the rods structure of Pal can be controlled by controlling the mass ratio of Pal to Fe_3O_4. When the mass ratio of Pal to Fe_3O_4 is 1:2, the specific surface area of the composite is enlarged from 10.29 m^2/g to 40.73 m^2/g. Meanwhile, the Pal/Fe_3O_4 composite exhibited an optimal reflection loss of "40.41 dB at 4.80 GHz due to the enhanced interface polarization. Although Pal can promote the microwave absorption performance of magnetic particles, traditional magnetic materials are limited in their wide applications due to their high density, large thickness and narrow absorption bandwidth. Therefore, it is very important to develop ideal microwave absorbing materials with light weight, strong absorption capacity, wide absorption bandwidth and thin thickness. Typical conductive materials such as carbon nanotubes, graphene oxide and various conductive polymers meet the above requirements [76, 77]. For example, palygorskite/polyaniline (Pal/PANI) composites were prepared with Pal as the disperse agent and aniline as the precursor through in-situ polymerization [78]. Due to the directional dispersion of aniline by Pal, the obtained Pal/PANI composites display a cross-linked shell structure and the thickness of the polymer shell can be adjusted by controlling the content of Pal, which has a positive effect on microwave absorption performance of the materials. Fig. 10 showed TEM images and RL profiles of the Pal/PANI composites with different proportions. Although the surface of the sample Pal/PANI-1 has large amount of PANI, the polymer shell is quite uniform, with a thickness of about 60 nm (Fig. 10 (a)). When the content of PANI was increased, the polymer shell (Pal/PANI-2) became lighter in color and smaller in thickness (Fig. 10 (b)). This phenomenon was more pronounced in Pal/PANI-3 (Fig. 10

(c)). Therefore, the PANI coating on the Pal nanorods can be controlled by adjusting the content of Pal, thus optimizing the microwave absorption properties of the composites. The optimized sample shows a reflection loss (RL) value of -57.40 dB at 11.04 GHz, at a thickness of 2.41 mm.

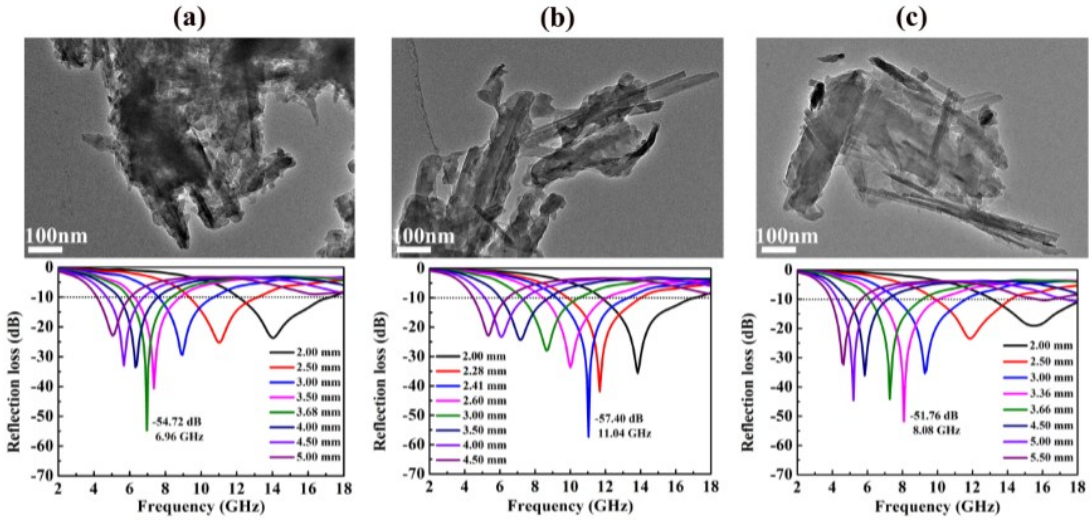

Fig. 10. TEM images and RL profiles of the composites: (a) Pal/PANI-1, (b) Pal/PANI-2 and (c) Pal/PANI-3 [76].

On this basis, we have developed the spherical shell shaped ternary microwave absorbers. The palygorskite/carbon (Pal/C) composites were prepared by using hydrothermal reaction with palygorskite and glucose as precursors. Then, the Pal/C composites, were used as a template to load polyaniline through in-situ polymerization, thus obtaining dispersed spherical shell-shaped palygorskite/carbon/polyaniline (Pal/C/PANI) ternary composites [79]. As shown in Fig. 11, (Pal/C) acted as a skeleton and dispersion agent has a certain influence on the microstructure of the ternary composites, and the thickness of spherical shell can be controlled by adjusting the content of polyaniline. Due to the improved impedance matching and increased dielectric loss, the Pal/C/PANI composites display an optimal reflection loss of "74 dB at 6.24 GHz, with a maximum effective absorption bandwidth of 4.96 GHz, as shown in Fig. 12.

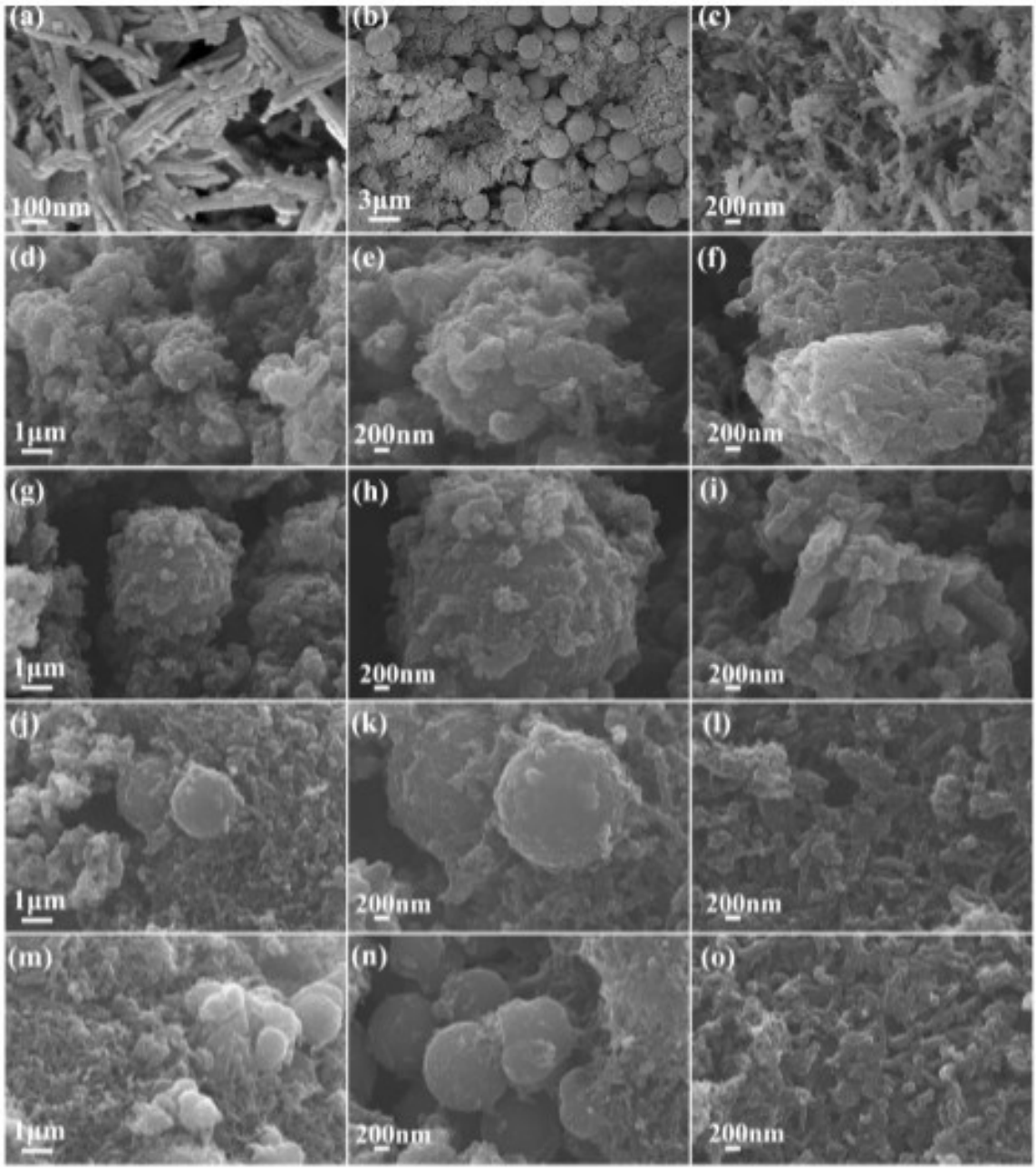

Fig. 11. FESEM images of different samples: (a) Pal, (b, c) Pal/C, (d, e, f) Pal/C/PANI-1, (g, h, i) Pal/C/PANI-2, (j, k, l) Pal/C/PANI-3 and (m, n, o) Pal/C/PANI-4 [79].

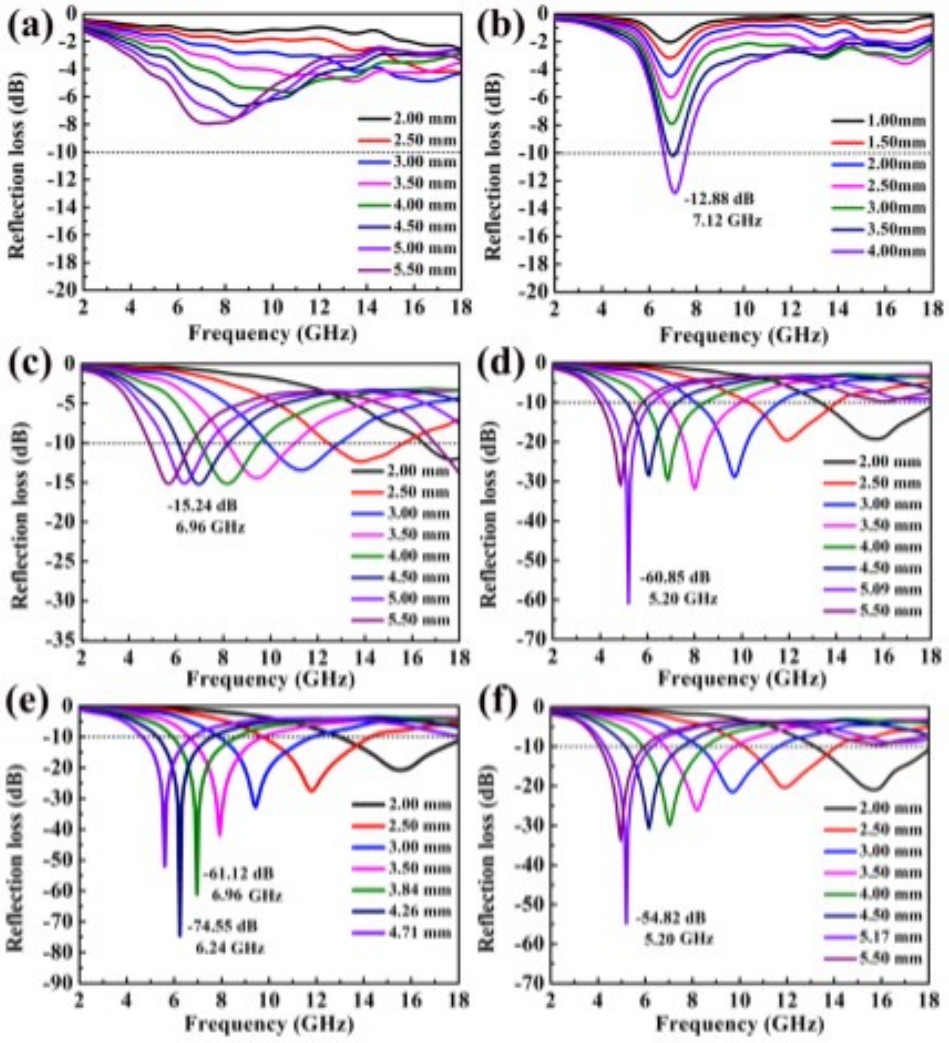

Fig. 12. Reflection loss curves of the samples at different thicknesses: (a) Pal, (b) Pal/C, (c) Pal/C/PANI-1, (d) Pal/C/PANI-2, (e) Pal/C/PANI-3 and (f) Pal/C/PANI-4 [79].

In addition, the performance of microwave absorbers can be optimized by adjusting the magnetic and dielectric parameters. For example, Ren et al prepared coral-like palygorskite-dispersed Fe_3O_4/polyaniline composites [80]. The possible loss mechanisms are proposed, as schematically depicted in Fig. 13. Excellent dielectric and magnetic characteristics of Fe_3O_4/PANI provide are mainly responsible for the strong electromagnetic absorption performance of the composites. Pal makes a significant contribution to the coral-like structure of the composites. Importantly, this special structure results in multiple reflections, scattering, interfacial polarization and improved impedance matching. Concurrently, the electromagnetic absorption performance of the Pal-dispersed Fe3O4/PANI is enhanced.

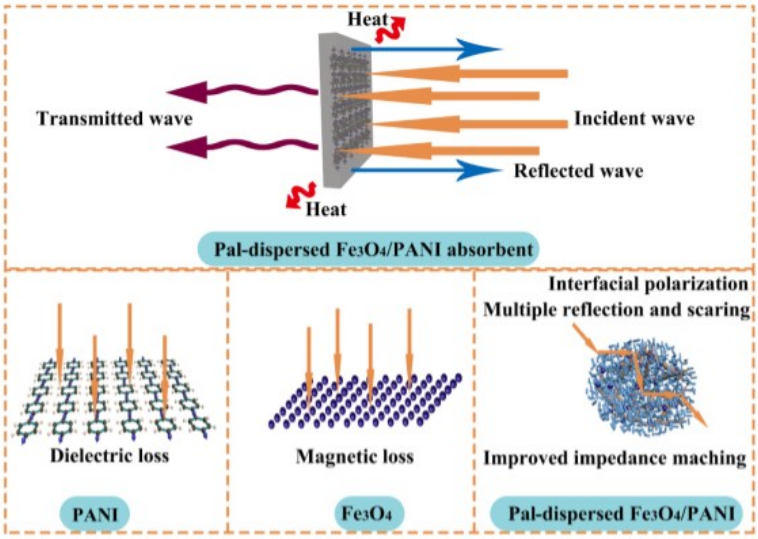

Fig. 13. Schematic illustration of potential electromagnetic loss mechanism for the Pal-dispersed Fe_3O_4/PANI [80].

4. Conclusions and perspectives

Palygorskite ((Pal) is a unique mineral with various special physical and chemical properties, which leads to a wide range of potential applications. However, for practical applications, purification and modification are required to ensure high performances. Various methods have been developed to purify and modify Pal clays. The potential applications include pollutant absorption, microwave absorption and photocatalysts. From these results, the adsorption capacity of Pal was not significantly improved by purification and dissociation. Pal based adsorbents were more dependent on the active functional groups inherent in the surface of Pal or grafted by various modification methods. However, Pal as a carrier in the field of photocatalysis and microwave absorption is more eager to purify and dissociate Pal. This is because the purified and dissociated Pal has higher specific surface area and more dispersed rod structure, which will greatly improve the dispersion of the loaded nanoparticles, and has an important impact on improving the light response and microwave loss. All in all, systematic study and deep understanding on the mechanisms of Pal as a carrier in the field of photocatalysis and microwave absorption have important reference and guiding significance for the future industrialization of Pal.

Author contributions

Liu, Y. and Zhang, T.S. provided the idea, Wang, S. wrote the paper, Kong, L.B. revised the paper, all authors were involved in the revision of the manuscript.

Conflicts of interest

The authors declare that they have no conflict of interest.

Acknowledgement

The authors gratefully acknowledge the financial support from supported by Foundation of State Key Laboratory of High-efficiency Utilization of Coal and Green Chemical Engineering (Grant No. 2021-K19), the Opening Project of State Key Laboratory of High Performance Ceramics and Superfine Microstructure (Grant Nos. SKL202003SIC), Anhui International Joint Research Center for Nano Carbon-based Materials and Environmental Health (No. 2020R0109). The Key Technologies R&D Program of Anhui Province of China (Grant No. 202104a05020033). The Shenzhen Technology University (SZTU) is acknowledged for the financial support of the Start-up Grant (2018) and Natural Science Foundation of Top Talent of SZTU (Grant No. 2019010801002).

References

[1] Suárez, M.; García-Romero, E. FTIR spectroscopic study of palygorskite: influence of the composition of the octahedral sheet. Applied Clay Science. **2006**, *31*, 154-163.

[2] Bradley, W.F. The structure scheme of attapulgite. American Mineralogist. **1940**, *25*, 405-410.

[3] Mckeown, D.A.; Post, J.E.; Etz, E.S. Vibrational analysis of palygorskite and sepiolite. Clays and Clay Minerals. **2002**, *50*, 667-680.

[4] Chiari, G.; Giustelto, R.; Ricchiardi, G. Crystal structure refinements of palygorskite and Maya Blue from molecular modeling and powder synchrotron dffraction. European Journal of Mineralogy. **2003**, *15*, 21-33.

[5] Post, J.E; Heaney, P.J. Synchrotron powder x-ray diffraction study of the structure and dehydration behavior of palygorskite. American Mineralogist. **2008**, *93*, 667-675.

[6] Wu, X.P.; Zhu, W.Y.; Zhang, X.L.; Chen, T.H.; Frost, R.L. Catalytic deposition of nanocarbon onto palygorskite and its adsorption of phenol. Applied Clay Science. **2011**, *52*, 400-406.

[7] Chen, H.; Zhao, J.; Zhong, A.G.; Jin, Y.X. Removal capacity and adsorption mechanism of heat-treated palygorskite clay for methylene blue. Chem. Eng. J. **2011**, *174*, 143-150.

[8] Singer, A. The texture of palygorskite from the Rift Valley, southern Israel. Clay Minerals. **1981**, *16*, 415-419.

[9] Garcia-Romero E.; Suárez, M. Sepiolite-palygorskite: textural study and genetic considerations. Applied Clay Science. **2013**, *86*, 129-144.

[10] Zhang, Y.L.; Zhao, J.; Chu, H.Q.; Zhou, X.F.; Wei, Y. Effect of modified attapulgite addition on the performance of a PVDF ultrafiltration membrane. Desalination. **2014**, *344*, 71-78.

[11] Jiang, L.P.; Liu, P.; Zhao, S.B. Magnetic ATP/FA/Poly(AA-co-AM) ternary nanocomposite microgel as selective adsorbent for removal of heavy metals from wastewater. Colloids and Surfaces A: Physicochemical and Engineering Aspects. *2015*, *470*, 31-38.

[12] Cao, J.L.; Shao, G.S.; Wang, Y.; Liu, Y.P.; Yuan, Z.Y. CuO catalysts supported on attapulgite clay for low-temperature CO oxidation. Catalysis Communications. *2008*, *9*, 2555-2559.

[13] Frost, R.L.; Xi, Y.F.; He, H.P. Synthesis, characterization of palygorskite supported zero-valent iron and its application for methylene blue adsorption. Journal of Colloid and Interface Science. **2010**, *341*, 153-161.

[14] Wang, W.B.; Wang, A.Q. Recent progress in dispersion of palygorskite crystal bundles for nanocomposites. Applied Clay Science. **2016**, *119*, 18-30.

[15] Boudriche, L.; Chamayou, A.; Calvet, R.; Hamdi, B.; Balard, H. Influence of different dry milling processes on the properties of an attapulgite clay, contribution of inverse gas chromatography. Powder Technology. **2014**, *254*, 352-363.

[16] Liu, Y.; Wang, W.B.; Wang,A.Q. Effect of dry grinding on the microstructure of palygorskite and adsorption effificiency for methylene blue. Powder Technology. **2012**, *225*, 124-129.

[17] Xu, J.X.; Zhang, J.P.; Wang, Q.; Wang, A.Q. Disaggregation of palygorskite crystal bundles via high-pressure homogenization. Applied Clay Science. **2011**, *54*, 118–123.

[18] Xu, J.X.; Wang, W.B.; Wang, A.Q. Enhanced microscopic structure and properties of palygorskite by associated extrusion and high-pressure homogenization process. Applied Clay Science. **2014**, *95*, 365-370.

[19] Chen, J.; Jin, Y.L.; Qian, Y.H.; Hu, T. New approach to efficiently disperse aggregated palygorskite into single crystals via adding freeze process into traditional extrusion treatment. IEEE Transactions on Nanotechnology, **2010**, *9*, 6-10.

[20] Xu, J.X.; Wang, W.B.; Wang, A.Q. A novel approach for dispersion palygorskite aggregates into nanorods via adding freezing process into extrusion and homogenization treatment. Powder Technology. **2013**, *249*, 157-162.

[21] Cai, D.Q.; Zhang, H.; Tang, Y.; Chu, P.K.; Yu, Z.L.; Wu, Z.Y.; Nano-networks have better adsorption capability than nano-rods. Nano Communication Networks. **2010**, *1*, 257-263.

[22] Zhang, J.; Cai, D.Q.; Zhang, G.L.; Cai, C.J.; Zhang, C.L.; Qiu, G.N.; Zheng, K.; Wu, Z.Y. Adsorption of methylene blue from aqueous solution onto multiporous palygorskite modified by ion beam bombardment: effect of contact time, temperature, pH and ionic strength. Applied Clay Science. **2013**, *83*, 137-143.

[23] Wang, S.; Ren, H.D.; Lian, W.; Wang, J.Z.; Zhao, Y.; Liu, Y.; Zhang, T.S.; Kong, L.B. Purification and dissociation of raw palygorskite through wet ball milling as a carrier to enhance the microwave absorption performance of Fe_3O_4. Applied Clay Science. **2021**, *200*, 105915.

[24] Frost, R.L.; Cash, G.A.; Kloprogge, J.T. 'Rocky Mountain leather', sepiolite and attapulgite-An infrared emission spectroscopic study. Vibrational Spectroscopy. **1998**, *16*, 173-184.

[25] Khorami, J.; Lemieux, A. Comparison of attapulgites from different sources using TG/DTG and FTIR. Thermochimica Acta. **1989**, *138*, 97-105.

[26] Frost, R. L.; Ding, Z. Controlled rate thermal analysis and differential scanning calorimetry of sepiolites and palygorskites. Thermochimica Acta. **2003**, *397*, 119-128.

[27] Boudriche, L.; Calvet, R.; Hamdi, B.; Balard, H. Surface properties evolution of attapulgite by IGC analysis as a function of thermal treatment. Colloids and Surfaces A: Physicochemical and Engineering Aspects. **2012**, *399*, 1-10.

[28] Chen, T.H.; Wang, J.; Qing, C.S.; Peng, S.C.; Song, Y.X.; Guo, Y. Effect of heat treatment on structure morphology and surface properties of palygorskite. Journal of the Chinese Ceramic Society. **2006**, *34*, 1406-1410 (in Chinese).

[29] Ye, H.P.; Chen, F.Z.; Sheng, Y.Q.; Sheng, G.Y.; Fu, J.M. Adsorption of phosphate from aqueous solution onto modified palygorskites. Separation and Purification Technology. **2006**, *50*, 283-290.

[30] Kuang, W.X.; Facey, G.A.; Detellier, C. Dehydration and rehydration of palygorskite and the influence of water on the nanopores. Clays and Clay Minerals. **2004**, *52*, 635-642.

[31] Frini-Srasra, N.; Srasra, E. Effect of heating on palygorskite and acid treated palygorskite properties. Surface Engineering and Applied Electrochemistry. **2008**, *44*, 43-49.

[32] Boudriche, L.; Calvet, R.; Hamdi, B.; Balard, H. Effect of acid treatment on surface properties evolution of attapulgite clay: An application of inverse gas chromatography. Colloids & Surfaces A Physicochemical & Engineering Aspects. **2011**, *392*, 45-54.

[33] Wang, W.B.; Dong, W.K.; Tian, G.Y.; Sun, L.Y.; Wang, Q.; Hui, A.P.; Mu, B.; Wang, A.Q. Highly efficient self-template synthesis of porous silica nanorods from natural palygorskite. Powder Technology. **2019**, *354*, 1-10.

[34] Ding, J.J.; Huang, D.J.; Wang, W.B.; Wang, Q .; Wang, A.Q. Effect of removing coloring metal ions from the natural brick-red palygorskite on properties of alginate/palygorskite nanocomposite film.

International Journal of Biological Macromolecules. **2019**, *122*, 684-694.

[35] Lai, S.Q.; Yue, L.; Zhao, X.F.; Gao, L.G. Preparation of silica powder with high whiteness from palygorskite. Applied Clay Science. **2010**, *50*, 432-437.

[36] Steudel, A.; Batenburg, L.F.; Fischer, H.R.; Weidler, P.G.; Emmerich, K. Alteration of swelling clay minerals by acid activation. Applied Clay Science. **2009**, *44*, 105-115.

[37] Wang, W.B.; Wang, F.F.; Kang, Y.R.; Wang, A.Q. Enhanced adsorptive removal of Methylene Blue from aqueous solution by alkali-activated palygorskite. Water Air and Soil Pollution. **2015**, *226*, 83.

[38] Huang, J.H.; Liu, Y.F.; Jin, Q.Z.; Wang, X.G.; Yang, J. Adsorption studies of a water soluble dye, reactive red MF-3B, using sonication-surfactant-modified attapulgite clay. Journal of Hazardous Materials. **2007**, *143*, 541-548.

[39] Huang, J.H.; Wang, X.G.; Jin, Q.Z.; Liu, Y.F.; Wang, Y. Removal of phenol from aqueous solution by adsorption onto OTMAC-modified attapulgite. Journal of Environmental Management. **2007**, *84*, 229-236.

[40] Dong, R.; Liu, Y.F.; Wang, X.G.; Huang, J.H. Adsorption of Sulfate Ions from aqueous solution by surfactant-modified palygorskite. Journal of Chemical & Engineering Data. **2011**, *56*, 3890-3896.

[41] Sarkar, B.; Xi, Y.F.; Megharaj, M.; Naidu, R. Orange II adsorption on palygorskites modified with alkyl trimethylammonium and dialkyl dimethylammonium bromide An isothermal and kinetic study. Applied Clay Science. **2011**, *51*, 370-374.

[42] Huang, J.H.; Liu, Y.F.; Wang, X.G. Selective adsorption of tannin from flavonoids by organically modified attapulgite clay. Journal of Hazardous Materials. **2008**, *160*, 382-387.

[43] Lei, Z.P.; Liu, Y.S.; Su, Z.X. Synthesis and characterization of organo-attapulgite/polyaniline-dodecylbenzenesulfonic acid based on emulsion polymerization method. Polymer Composites. **2008**, *29*, 239-244.

[44] Xu, J.X.; Kang, Y.R.; Wang, A.Q. Effects of sodium oleate on physicochemical properties of the modified attapulgite. China Mining Magazine. **2011**, *20*, 102-105(in Chinese).

[45] Xue, A.L.; Zhou, S.Y.; Zhao, Y.J.; Lu, X.P.; Han, P.F. Effective NH_2-grafting on attapulgite surfaces for adsorption of reactive dyes. Journal of Hazardous Materials. **2011**, *194*, 7-14.

[46] Peng, Y. G.; Chen, D.J.; Ji, J.L.; Kong, Y.; Wan, H.X.; Yao, C. Chitosan-modified palygorskite: Preparation, characterization and reactive dye removal. Applied Clay Science. **2013**, *74*, 81-86.

[47] Liu, P.; Guo, J.S. Polyacrylamide grafted attapulgite (PAM-ATP) via surface-initiated atom transfer radical polymerization (SI-ATRP) for removal of Hg(II) ion and dyes. Colloids and Surfaces A: Physicochemical and Engineering Aspects. **2006**, *282*, 498-503.

[48] Sonmez, H.B.; Senkal, B.F.; Sherrington, D.C.; Býcak, N. Atom transfer radical graft polymerization of acrylamide from N-chlorosulfonamidated polystyrene resin, and use of the resin in selective mercury removal. Reactive and Functional Polymers. **2003**, *55*, 1-8.

[49] Chen, T.H.; Liu, H.B.; Li, J.H.; Chen, D.; Chang, D.Y.; Kong, D.J.; Frost, R.L. Effect of thermal treatment on adsorption–desorption of ammonia and sulfur dioxide on palygorskite: Change of surface acid–alkali properties. Chemical Engineering Journal. **2011**, *166*, 1017-1021.

[50] Frini-Srasra, N.; Srasra, E. Acid treatment of south Tunisian palygorskite: Removal of Cd(II) from aqueous and phosphoric acid solutions. Desalination. **2010**, *250*, 26-34.

[51] Chen, H.; Zhao, Y.G.; Wang, A.Q. Removal of Cu(II) from aqueous solution by adsorption onto acid-activated palygorskite. Journal of Hazardous Materials. **2007**, *149*, 346-354.

[52] Wang, Y. Q.; Feng, Y.; Zhang, X.F.; Zhang, X.G.; Jiang, J.L.; Yao, J.F. Alginate-based attapulgite foams as efficient and recyclable adsorbents for the removal of heavy metals. Journal of Colloid and Interface Science. **2018**, *514*, 190-198.

[53] Mao, X.Y.; Wang, L.; Gu, S.Q.; Duan, Y.Y.; Zhu, Y.Q.; Wang, C.Y.; Lichtfouse, E. Synthesis of a three-dimensional network sodium alginate-poly(acrylic acid)/attapulgite hydrogel with good mechanic property and reusability for efficient adsorption of Cu^{2+} and Pb^{2+}. Environmental Chemistry Letters.

2018, *16*, 653-658.

[54] Cui, H.; Qian, Y.; Li, Q.; Zhang, Q.; Zhai, J.P.Adsorption of aqueous Hg(II) by a polyaniline/attapulgite composite. Chemical Engineering Journal. **2012**, *211*, 216-223.

[55] Liu, Y.; Wang, W.B.; Wang, A.Q. Adsorption of lead ions from aqueous solution by using carboxymethyl cellulose-g-poly (acrylic acid)/attapulgite hydrogel composites. Desalination. **2010,** *259*, 258-264.

[56] Chen. H.; Wang. A.Q. Adsorption characteristics of Cu(II) from aqueous solution onto poly(acrylamide)/attapulgite composite. Journal of Hazardous Materials. **2009**, *165*, 223-231.

[57] Tian, G.Y.; Wang, W.B.; Kang, Y.R.; Wang, A.Q. Palygorskite in sodium sulphide solution via hydrothermal process for enhanced methylene blue adsorption. Journal of the Taiwan Institute of Chemical Engineers. **2016**, *58*, 417-423.

[58] Wang, X.H.; Zheng, Y.; Wang, A.Q. Fast removal of copper ions from aqueous solution by chitosan-g-poly(acrylic acid)/attapulgite composites. Journal of Hazardous Materials. **2009**, *168*, 970-977.

[59] Bhattacharya, A.K.; Mandal, S.N.; Das, S.K. Adsorption of Zn(II) from aqueous solution by using different adsorbents. Chemical Engineering Journal. **2006**, *123*, 43-51.

[60] Fan, Q.H.; Li, Z.; Zhao, H.G.; Jia, Z.H.; Xu, J.Z.; Wu, W.S. Adsorption of Pb(II) on palygorskite from aqueous solution: Effects of pH, ionic strength and temperature. Applied Clay Science. **2009**, *45*, 111-116.

[61] Moreira, M.A.; Ciuffi, K.J.; Rives, V.; Vicente, M.A.; Trujillano, R.; Gil, A.; Korili, S.A.; de Faria, E.H. Effect of chemical modification of palygorskite and sepiolite by 3-aminopropyltriethoxisilane on adsorption of cationic and anionic dyes. Applied Clay Science. **2017**, *135*, 394-404.

[62] Kausar, A.; Iqbal, M.; Javed, A.; Aftab, K.; Nazli, Z.I.H.; Bhatti, H.N.; Nouren, S. Dyes adsorption using clay and modified clay: A review. Journal of Molecular Liquids. **2018**, *256*, 395-407.

[63] Papoulis; D.; Komameni, S.; Panagiolaras, D.; Nikolopoulou, A.;Li, H.H.; Yin, S.; Tsugio, S.; Katsuki, H. Palygorskite-TiO_2 nanocomposites. Part 1. Synthesis and characterization. Applied Clay Science. **2013**, *83*, 191-197.

[64] Papoulis, D.; Komarneni, S.; Nikolopoulou, A.; Tsolis-Katagas, P.; Panagiotaras, D.; Kacandes, G.H.; Zhang, P.; Yin, S.; Sato, T.; Katsuki, H. Palygorskite and halloysite-TiO_2 nanocomposites: synthesis and photocatalytic activity. Applied Clay Science. **2010**, *50*, 118-124.

[65] Huo, C.L.; Yang, H.M. Preparation and enhanced photocatalytic activity of Pd-CuO/palygorskite nanocomposites. Applied Clay Science. **2013**, *74*, 87-94.

[66] Liu, Z.S.; Bi, Y.H.; Zhao, Y.L.; Huang, X.; Zhu, Y.B. Synthesis and photocatalytic property of BiOBr/palygorskite composites. Materials Research Bulletin. **2014**, *49*, 167-171.

[67] Chen, D.M.; Du, Y.; Zhu, H.L.; Deng, Y.X. Synthesis and characterization of a microfibrous TiO_2-CdS/palygorskite nanostructured material with enhanced visible light photocatalytic activity. Applied Clay Science. **2014**, *87*, 285-291.

[68] Zhang, G.K.; Wang, H.; Guo, S.; Wang, J.T.; Liu, J. Synthesis of Cu/TiO_2/organo-attapulgite fiber nanocomposite and its photocatalytic activity for degradation of acetone in air. Applied Surface Science, **2016**, *362*, 257-264.

[69] Ma, J.F.; Zou, J.; Li, L.Y.; Yao, C.; Kong, Y.; Cui, B.; Zhu, R.L.; Li, D.L. Nanocomposite of attapulgite-Ag_3PO_4 for Orange II photodegradation. Applied Catalysis B: Environmental. Applied Clay Science. **2014**, *144*, 36-40.

[70] Wang, X.W.; Mu, B.; An, X.C.; Wang, A.Q. Insights into the relationship between the color and photocatalytic property of attapulgite/CdS nanocomposites. Applied Surface Science. **2018**, *439*, 202-212.

[71] Li, X.Y.; Peng, K. Hydrothermal synthesis of MoS_2 nanosheet/palygorskite nanofiber hybrid nanostructures for enhanced catalytic activity. Applied Clay Science. **2018**, *87*, 175-181.

[72] Wang, S.; Wang, Y.; Zhuang, Y.; Lian, W.; Ren, H.D.; Liu, Y.; Zhang, T.S.; Kong, L.B. Synthesis of

palygorskite supported spherical ZnS nanocomposites with enhanced photocatalytic activity. CrystEngComm. **2021**, *23*, 4229-4236.

[73] Luo, J.; Luo, Y.T.; Yang, J.C.; Zhang, M.; Chen, S.M.; Liu, X.H. Composite microsphere resulting from assembly of BiOCl nanosheets and palygorskite nanorods for enhanced photocatalytic activity. Applied Clay Science. **2019**, *168*, 450-458.

[74] Shu, X.F.; Zhou, J.; Liu, Y.; Wang, Y.Q.; Hu, B.; Jiang, Y.; Kong, L.B.; Zhang, T.S.; Song, H.X. Hollow Fe_3O_4 microspheres/graphene composites with adjustable electromagnetic absorption properties, Diamond and Related Materials. **2019**, *97*, 107441.

[75] Shang, T.; Lu, Q.S.; Chao, L.M.; Qin, Y.L.; Yun, Y.H.; Yun, G.H. Effects of ordered mesoporous structure and La-doping on the microwave absorbing properties of $CoFe_2O_4$. Applied Surface Science. **2018**, *434*, 234-242.

[76] Sun, X.; He, J.; Guoxian, l.; Tang, J.; Wang, T.; Guo, Y.; Xue, H. Laminated magnetic graphene with enhanced electromagnetic wave absorption properties. Journal of Materials Chemistry C. **2012**, *1*, 765-777.

[77] Luo, J.; Zhang, K.; Cheng, M.; Gu, M.; Sun, X. MoS_2 spheres decorated on hollow porous ZnO microspheres with strong wideband microwave absorption. Chemical Engineering Journal. **2019**, *380*, 122625.

[78] Wang, S.; Lian, W.; Ren, H.D.; Ma, J.L.; Liu, Y.; Zhang, T.S.; Kong, L.B. Novel composites with a cross-linked polyaniline shell and oriented palygorskite as ideal microwave absorbers. New Journal of Chemistry. **2021**, *45*, 2765-2774.

[79] Wang, S.; Ren, H.D.; Lian, W.; Zhang, X.M.; Liu, Z.Y.; Liu, Y.; Zhang, T.S.; Kong, L.B.; Bai, H.C. Dispersed spherical shell-shaped palygorskite/carbon/polyaniline composites with advanced microwave absorption performances. Powder Technology. **2021**, *387*, 277-286.

[80] Ren, H.D.; Wang, S.; Lian, W.; Ma, J.L.; Zhao, Y.; Liu, Y.; Zhang, T.S.; Kong, L.B.; Oh, W.C. Preparation of coral-like palygorskite-dispersed Fe_3O_4/polyaniline with improved electromagnetic absorption performance. Applied Clay Science. **2021**, *204*, 106009.